

AD-A 130 293

TECHNICAL
LIBRARY

AD

TECHNICAL REPORT ARBRL-TR-02495

NUMERICAL COMPUTATION OF BASE FLOW FOR A
PROJECTILE AT TRANSONIC SPEEDS

Jubaraj Sahu
Charles J. Nietubicz
Joseph L. Steger

June 1983

DTIC QUALITY INSPECTED 2



US ARMY ARMAMENT RESEARCH AND DEVELOPMENT COMMAND
BALLISTIC RESEARCH LABORATORY
ABERDEEN PROVING GROUND, MARYLAND

Approved for public release; distribution unlimited.

Destroy this report when it is no longer needed.
Do not return it to the originator.

Additional copies of this report may be obtained
from the National Technical Information Service,
U. S. Department of Commerce, Springfield, Virginia
22161.

The findings in this report are not to be construed as
an official Department of the Army position, unless
so designated by other authorized documents.

*The use of trade names or manufacturers' names in this report
does not constitute indorsement of any commercial product.*

UNCLASSIFIED

SECURITY CLASSIFICATION OF THIS PAGE (When Data Entered)

REPORT DOCUMENTATION PAGE		READ INSTRUCTIONS BEFORE COMPLETING FORM
1. REPORT NUMBER TECHNICAL REPORT ARBRL-TR-02495	2. GOVT ACCESSION NO.	3. RECIPIENT'S CATALOG NUMBER
4. TITLE (and Subtitle) NUMERICAL COMPUTATION OF BASE FLOW FOR A PROJECTILE AT TRANSONIC SPEEDS		5. TYPE OF REPORT & PERIOD COVERED Final
		6. PERFORMING ORG. REPORT NUMBER
7. AUTHOR(s) J. Sahu, C.J. Nietubicz, and J.L. Steger*		8. CONTRACT OR GRANT NUMBER(s)
9. PERFORMING ORGANIZATION NAME AND ADDRESS U.S. Army Ballistic Research Laboratory ATTN: DRDAR-BLL Aberdeen Proving Ground, Maryland 21005		10. PROGRAM ELEMENT, PROJECT, TASK AREA & WORK UNIT NUMBERS 1L161102AH43
11. CONTROLLING OFFICE NAME AND ADDRESS US Army Armament Research & Development Command US Army Ballistic Research Laboratory (DRDAR-BLA-S) Aberdeen Proving Ground, MD 21005		12. REPORT DATE June 1983
		13. NUMBER OF PAGES 33
14. MONITORING AGENCY NAME & ADDRESS (if different from Controlling Office)		15. SECURITY CLASS. (of this report) Unclassified
		15a. DECLASSIFICATION/DOWNGRADING SCHEDULE
16. DISTRIBUTION STATEMENT (of this Report) Approved for public release, distribution unlimited.		
17. DISTRIBUTION STATEMENT (of the abstract entered in Block 20, if different from Report)		
18. SUPPLEMENTARY NOTES *Stanford University Department of Aeronautics and Astronautics ATTN: Prof. J. Steger Stanford, CA 94305		
19. KEY WORDS (Continue on reverse side if necessary and identify by block number) Navier-Stokes Computation Base Pressure Base flow Projectile Aerodynamics Transonic speeds Drag Components		
20. ABSTRACT (Continue on reverse side if necessary and identify by block number) The Generalized-Axisymmetric Thin-Layer Navier-Stokes computational technique has been modified for projectile base flow analysis. The resulting new numerical capability is used to compute the entire projectile flow field including the recirculatory base flow. Computed results show the qualitative and quantitative details of the overall base flow structure. Base drag is computed for a secant-ogive-cylinder projectile at an angle of attack of zero and compared with available experimental data and a semi-empirical analysis. Results are also presented which show pressure drag, skin friction drag and total aerodynamic drag for Mach No. $.9 < M < 1.2$.		

TABLE OF CONTENTS

	<u>Page</u>
LIST OF ILLUSTRATIONS.....	5
I. INTRODUCTION.....	7
II. GOVERNING EQUATIONS.....	8
III. NUMERICAL METHOD.....	11
A. Computational Algorithm.....	11
B. Finite Difference Equations.....	11
C. Flow Field Segmentation.....	12
D. Implementation of Boundary Conditions.....	13
IV. RESULTS.....	14
V. SUMMARY.....	17
REFERENCES.....	27
LIST OF SYMBOLS.....	29
DISTRIBUTION LIST.....	31

LIST OF ILLUSTRATIONS

<u>Figure</u>		<u>Page</u>
1	Spark Shadowgraph of Secant-Ogive-Cylinder-Boattail Projectile, M = 0.95, $\alpha \approx 0$	18
2	Axisymmetric Body and Coordinate System.....	18
3	Schematic Illustration of Flow Field Segmentation.....	19
4	Model Geometry.....	19
5	Computational Grid for Flow Field Computations.....	20
6	Expanded Grid.....	20
7	Longitudinal Surface Pressure Distribution, M = 0.9, $\alpha = 0$	21
8	Longitudinal Surface Pressure Distribution, M = 0.9, $\alpha = 0$	21
9	Velocity Vector Field, M = 0.9, $\alpha = 0$	22
10	Velocity Vector Field, M = 0.9, $\alpha = 0$	22
11	Velocity Vector Field, M = 0.9, $\alpha = 0$	23
12	Stream Function Contours, M = 0.9, $\alpha = 0$	23
13	Stream Function Contours, M = 0.9, $\alpha = 0$	24
14	Variation of Base Drag Coefficient with Mach Number, $\alpha = 0$	24
15	Variation of Pressure Drag Coefficient with Mach Number, $\alpha = 0$...	25
16	Variation of Viscous Drag Coefficient with Mach Number, $\alpha = 0$	25
17	Variation of Total Drag Coefficient with Mach Number, $\alpha = 0$	26

I. INTRODUCTION

New computational algorithms together with advances in computer resources are beginning to show promise as viable predictive capabilities for the aerodynamics of projectiles. Recent papers^{1,2} have reported the development and application of the Azimuthal-Invariant Thin-Layer Navier-Stokes computational technique to predict the flow about slender bodies of revolution at transonic speeds. References 1 and 2 showed the technique to be a viable computational tool for predicting both external and internal flows for spinning and non-spinning bodies of various geometric shapes. These calculations, however, modeled the base flow as an extended sting and thus the base pressure and recirculatory base flow were not computed. Only until very recently with the advent of LDV instrumentation are reliable base flow data becoming available. Therefore, only a very limited amount of data are presently available and in general are usually in terms of overall drag data rather than specific base pressure data.

The base flow problem at supersonic speeds has been an area of extensive research. An excellent review of base drag is presented in Reference 3. Recently, Navier-Stokes solvers^{4,5} have been used to compute the aft end flow field of axisymmetric bodies at supersonic velocities. At transonic speeds, a limited study of the flow past a boattailed afterbody has been performed by Chow, et. al.⁶ The inviscid transonic flow is solved by finite difference calculations of the axisymmetric potential equation, and the viscous flow behind the base is treated through integral formulations. This report

-
1. Nietubicz, C.J., Pulliam, T.H., and Steger, J.L., "Numerical Solution of the Azimuthal-Invariant Thin-Layer Navier-Stokes Equations," ARBRL-TR-02227, U.S. Army Ballistic Research Laboratory, ARRADCOM, Aberdeen Proving Ground, MD 21005, March 1980 (AD A085716).
 2. Nietubicz, C.J., "Navier-Stokes Computations for Conventional and Hollow Projectile Shapes at Transonic Velocities," AIAA Paper No. 81-1262, June 1981.
 3. Sedney, R., "Review of Base Drag," U.S. Army Ballistic Research Laboratory, ARRADCOM, Report No. 1337, Aberdeen Proving Ground, MD 21005, October 1966 (AD 808767).
 4. Diewert, G.S., "A Computational Investigation of Supersonic Axisymmetric Flow over Boattails Containing a Centered Propulsive Jet," AIAA Paper No. 83-0462, January 10-13, 1983.
 5. Weinberg, B.C., McDonald, H., and Shamroth, S.J., "Navier-Stokes Computations of Aft End Flow Fields," Final Report, Army Research Office Contract DAAG29-79-C-0003, May 1982.
 6. Chow, W.L., Bober, L.J., and Anderson, B.H., "Strong Interaction Associated with Transonic Flow Past Boattails," *AIAA Journal*, Vol. 13, No. 1, 1975, pp. 112-113.

describes a new numerical capability to compute the flow field in the base region of projectiles at transonic speeds and thus the total aerodynamic drag can now be computed.

The total drag for projectiles can be divided into three components: (1) pressure (wave) drag, (2) viscous (skin friction) drag, and (3) base drag. For a typical shell at $M = .9$, the relative magnitudes of the aerodynamic drag components are: (1) pressure drag, 20%; (2) viscous drag, 30%; and (3) base drag, 50%. In order to predict the total drag for projectiles, computation of the full flow field (including the base flow) must be made. Computation of base flow is especially important at transonic speeds.

The critical aerodynamic behavior of projectiles occurs in the transonic speed regime. This can be attributed to the complex shock structure which exists for the projectiles at transonic speeds. Figure 1 is a spark shadow-graph which shows the shock structure for a typical projectile at $M = .95$, $\alpha \approx 0$. It also shows a clearly defined wake behind the base of the projectile devoid of any vortex shedding. In the present effort primary emphasis is on the base region flow field computations; however, the technique used computes the full flow field over the projectile (including the base region). Therefore, all three components of the drag are computed.

A brief description of the governing equations and the method of solution are given in Sections II and III. A unique flow field segmentation procedure and the implementation of boundary conditions are discussed in Section III. In Section IV computed results are given for transonic flow about a 6-caliber secant-ogive-cylinder shape for $.9 < M < 1.2$, $\alpha = 0$. Velocity vector plots and stream function contour plots are presented to show the qualitative features of the flow field in the base region. All three components of drag are obtained. Base drag is compared with experimental and semi-empirical data while the total drag is compared with available semi-empirical data. The encouraging results show that the present computational technique can be successfully used to predict the base region flow field of projectiles. The results reported here are for transonic speeds, but future computational efforts using the same technique will be directed at supersonic velocities.

II. GOVERNING EQUATIONS

The Azimuthal Invariant (or Generalized Axisymmetric) thin-layer Navier-Stokes equations for general spatial coordinates ξ , η , ζ can be written as¹

$$\partial_{\tau} \hat{q} + \partial_{\xi} \hat{E} + \partial_{\zeta} \hat{G} + \hat{H} = \text{Re}^{-1} \partial_{\zeta} \hat{S} \quad (1)$$

where $\xi = \xi(x,y,z,t)$ is the longitudinal coordinate
 $\eta = \eta(y,z,t)$ is the circumferential coordinate
 $\zeta = \zeta(x,y,z,t)$ is the near normal coordinate
 $\tau = t$ is the time

The notation for the physical coordinates x, y, z , and the transformed coordinates ξ, η, ζ are shown in Figure 2. The vector of dependent variables \hat{q} and the flux vectors $\hat{E}, \hat{G}, \hat{H}$ are given as

$$\hat{q} = J^{-1} \begin{bmatrix} \rho \\ \rho u \\ \rho v \\ \rho w \\ e \end{bmatrix}, \quad \hat{E} = J^{-1} \begin{bmatrix} \rho U \\ \rho u U + \xi_x p \\ \rho v U + \xi_y p \\ \rho w U + \xi_z p \\ (e+p)U - \xi_t p \end{bmatrix}, \quad \hat{G} = J^{-1} \begin{bmatrix} \rho W \\ \rho u W + \zeta_x p \\ \rho v W + \zeta_y p \\ \rho w W + \zeta_z p \\ (e+p)W - \zeta_t p \end{bmatrix},$$

$$\hat{H} = J^{-1} \phi_\eta \begin{bmatrix} 0 \\ 0 \\ \rho V [R_\xi (U - \xi_t) + R_\zeta (W - \zeta_t)] \\ -\rho V R_\eta (V - \eta_t) - p / (R \phi_\eta) \\ 0 \end{bmatrix}$$

The thin layer viscous terms valid for high Reynolds number flow are contained in the vector \hat{S} , where

$$\hat{S} = \begin{bmatrix} 0 \\ \mu(\zeta_x^2 + \zeta_y^2 + \zeta_z^2)u_\zeta + (\mu/3)(\zeta_x u_\zeta + \zeta_y v_\zeta + \zeta_z w_\zeta)\zeta_x \\ \mu(\zeta_x^2 + \zeta_y^2 + \zeta_z^2)v_\zeta + (\mu/3)(\zeta_x u_\zeta + \zeta_y v_\zeta + \zeta_z w_\zeta)\zeta_y \\ \mu(\zeta_x^2 + \zeta_y^2 + \zeta_z^2)w_\zeta + (\mu/3)(\zeta_x u_\zeta + \zeta_y v_\zeta + \zeta_z w_\zeta)\zeta_z \\ \{(\zeta_x^2 + \zeta_y^2 + \zeta_z^2)[0.5\mu(u^2 + v^2 + w^2)_\zeta + \kappa Pr^{-1}(\gamma - 1)^{-1}(a^2)_\zeta] \\ + (\mu/3)(\zeta_x u + \zeta_y v + \zeta_z w)(\zeta_x u_\zeta + \zeta_y v_\zeta + \zeta_z w_\zeta)\} \end{bmatrix}$$

The velocities

$$\begin{aligned}
U &= \xi_t + \xi_x u + \xi_y v + \xi_z w \\
V &= \eta_t + \eta_x u + \eta_y v + \eta_z w \\
W &= \zeta_t + \zeta_x u + \zeta_y v + \zeta_z w
\end{aligned}
\tag{2}$$

represent the contravariant velocity components.

The Cartesian velocity components (u,v,w) are nondimensionalized with respect to a_∞ (the free stream speed of sound). The density (ρ) is referenced to ρ_∞ and total energy (e) to $\rho_\infty a_\infty^2$. The local pressure is determined using the equation of state,

$$p = (\gamma-1)[e - 0.5\rho(u^2+v^2+w^2)] \tag{3}$$

where γ is the ratio of specific heats.

In high Reynolds number flows the thin-layer approximation is often used because, due to computer speed and storage limitations, fine grid spacing can only be provided in one coordinate direction. This assumption has been validated for flows about various aerodynamic models but still remains a question in the wake region of bluff bodies. The grid spacing available in other directions is usually too coarse to resolve the viscous terms. Essentially, all the viscous terms in the coordinate direction ξ and η are neglected while terms in the near normal direction to the body ζ are retained. The thin-layer generalized axisymmetric equations (1) are obtained from the three dimensional equations by making use of two restrictions: (i) all body geometries are of an axisymmetric type; and (ii) the state variables and the contravariant velocities do not vary in the circumferential direction (η). Essentially, the η -derivative term in the three dimensional equations is replaced by a source term \hat{H} as it appears in equation (1). The details can be found in Reference 1 and 2.

Equation (1) contains only two spatial derivatives; however, it retains all three momentum equations, thus allowing a degree of generality over the standard axisymmetric equations. In particular, the circumferential velocity is not assumed to be zero, thus allowing computations for spinning projectiles or swirl flow to be accomplished.

For the computation of turbulent flows a turbulence model must be supplied. In the present calculations a Cebeci-type two layer algebraic eddy viscosity model as modified by Baldwin and Lomax⁷ is used. In their two-layer model the inner region follows the Prandtl-Van Driest formulation. Their outer formulation can be used in wakes as well as in attached and separated

7. Baldwin, B.S., and Lomax, H., "Thin-Layer Approximation and Algebraic Model for Separated Turbulent Flows," AIAA Paper No. 78-257, 1978.

boundary layers. In both the inner and outer formulations the distribution of vorticity is used to determine length scales, thereby avoiding the necessity of finding the outer edge of the boundary layer (or wake). The magnitude of the local vorticity for the axisymmetric formulation is given by

$$|\omega| = \sqrt{\left(\frac{\partial v}{\partial x}\right)^2 + \left(\frac{\partial v}{\partial z} - \frac{\partial w}{\partial y}\right)^2 + \left(\frac{\partial w}{\partial x} - \frac{\partial u}{\partial z}\right)^2} \quad (4)$$

III. NUMERICAL METHOD

A. Computational Algorithm

An implicit approximate factorization finite-difference scheme in delta form is used as described by Beam and Warming.⁸ An implicit method was chosen because it permits a time step much greater than that allowed by explicit schemes. For problems in which the transient solution is not of primary interest, this offers the possible advantage of being able to reach the steady state solution faster than existing explicit schemes.

The Beam-Warming implicit algorithm has been used in various applications.^{1,2,7-10} The algorithm can be first or second order accurate in time and second or fourth order accurate in space. The equations are factored (spatially split), which reduces the solution process to one-dimensional problems at a given time level. Central difference operators are employed and the algorithm produces block tridiagonal systems for each space coordinate. The main computational work is contained in the solution of these block tridiagonal systems of equations.

B. Finite Difference Equations

The resulting finite difference equations, written in delta form, are

-
8. Beam, R., and Warming, R.F., "An Implicit Factored Scheme for the Compressible Navier-Stokes Equations," *AIAA Paper No. 77-645*, June 1977.
 9. Steger, J.L., "Implicit Finite Difference Simulation of Flow About Arbitrary Geometries with Application to Airfoils," *AIAA Journal*, Vol. 16, No. 4, July 1978, pp. 679-686.
 10. Pulliam, T.H., and Steger, J.L., "On Implicit Finite-Difference Simulations of Three-Dimensional Flow," *AIAA Journal*, Vol. 18, No. 2, February 1980, pp. 159-167.

$$\begin{aligned}
& (I+h\delta_{\xi}\hat{A}^n-\epsilon_I J^{-1}\nabla_{\xi}\Delta_{\xi}J)(I+h\delta_{\zeta}\hat{C}^n-\epsilon_I J^{-1}\nabla_{\zeta}\Delta_{\zeta}J \\
& - hRe^{-1}\delta_{\zeta}J^{-1}\hat{M}^nJ) \times (\hat{q}^{n+1}-\hat{q}^n) = -\Delta t(\delta_{\xi}\hat{E}^n+\delta_{\zeta}\hat{G}^n \\
& -Re^{-1}\delta_{\zeta}\hat{S}^n)-\Delta t\hat{H}^n-\epsilon_E J^{-1}[(\nabla_{\xi}\Delta_{\xi})^2 + (\nabla_{\zeta}\Delta_{\zeta})^2]J\hat{q}^n
\end{aligned} \tag{5}$$

Here $h = \Delta t$ because only first order accuracy in the time differencing is needed for the steady state flows which are considered here. This choice corresponds to the Euler implicit time differencing. The δ 's represent central difference operators, Δ and ∇ are forward and backward difference operators respectively. The Jacobian matrices $\hat{A} = \frac{\partial \hat{E}}{\partial q}$, $\hat{C} = \frac{\partial \hat{G}}{\partial q}$ along with the coefficient matrix \hat{M} obtained from the local time linearization of \hat{S} are described in detail in Reference 10. Fourth order explicit (ϵ_E) and implicit (ϵ_I) numerical dissipation terms are incorporated into the differencing scheme to damp high frequency growth and thus to control the nonlinear instabilities. A typical range for the smoothing coefficients is $\epsilon_E = (1 \text{ to } 5) \Delta t$ with $\epsilon_I = 3\epsilon_E$.

C. Flow Field Segmentation

The objective of this report is to compute the full flow field of a projectile (including the base flow) at transonic speeds. This has been accomplished by a unique flow field segmentation procedure which is instrumental in the development of the current method for the computation of base flow. This segmentation is considered to be the main contribution to the state of art, as far as the computational algorithm is concerned. The segmentation significantly effects the treatment of boundary conditions and thus changes the internal structure of the block tridiagonal matrix. The details of these changes are described later.

Figure 3 is a schematic illustration of the flow field segmentation that is used to compute the entire projectile flow field including the base flow. It shows the transformation of the physical domain into the computational domain together with the details of the flow field segmentation procedure in both domains.

The cross hatched region represents the projectile. The line BC is the projectile base and the region ABCD is the base region or the wake. The line AB is a computational cut through the physical wake region which acts as a repetitive boundary in the computational domain. Implicit integration is carried out in both ξ and ζ directions. (See Figure 3.) Note the presence of the lines BC (the base) and EF (nose axis) in the computational domain. They both act as boundaries in the computational domain and special care must be taken in inverting the block tridiagonal matrix in the ξ direction.

flow variables are set equal to those at a grid point next to the base. Future work will be directed at the implementation of viscous boundary condition at the base to further evaluate this approximation.

Along the computational cut (line AB) the flow variables above and below the cut were simply averaged to determine the boundary conditions on the cut. On the center line of the wake region, a symmetry condition is imposed.

$$\begin{aligned}\frac{\partial u}{\partial z} &= 0 \\ \frac{\partial v}{\partial z} &= 0 \\ w &= 0 \\ \frac{\partial p}{\partial z} &= 0\end{aligned}\tag{8}$$

Free stream conditions are used at the outer boundary. First order extrapolation for all flow variables is used at the downstream boundary (lines AD and AG). During transient calculations, use of a specified outflow pressure can give rise to numerical oscillations in the base region flow field. Eventually, these grow and swamp the solution. This difficulty is avoided by simply extrapolating pressure to the downstream boundary, which is the procedure always used with supersonic outflow. A combination of extrapolation and symmetry is used at on the nose axis (line EF).

IV. RESULTS

A series of computations have been made for the 3-caliber (1 caliber \equiv 1 max. body diameter) secant-ogive nose and 3-caliber cylinder shape shown in Figure 4. All the computations were obtained for Mach numbers $.9 < M < 1.2$ and $\alpha = 0$. Limited base pressure measurements were made by Kayser¹¹ for this projectile shape and are compared with the computed results. The projectile was supported by a base-mounted sting and measurements of base pressure were made at only one location on the base. These experiments were conducted at Langley Research Center 8-foot Transonic Pressure Tunnel. Computed base pressures are also compared with available semi-empirical¹² data. The results are presented in the form of surface pressure distribution, contour plots and

11. Kayser, L.D., "private communications," Ballistic Research Laboratory, Aberdeen Proving Ground, MD 21005.

12. McCoy, R.L., "McDrag - A Computer Program for Estimating the Drag Coefficients of Projectiles," ARBRL-TR-02293, U.S. Army Ballistic Research Laboratory, ARRADCOM, Aberdeen Proving Ground, MD 21005, February 1981 (AD A098110).

velocity vector plots.

The computational grid used for the numerical computations was obtained from a versatile grid generator described in Reference 13. This program allows arbitrary grid point clustering, thus enabling grid points for the projectile shapes to be clustered in the vicinity of the body surface. The grid consists of 108 points in the longitudinal direction and 50 points in the radial direction. The full grid is shown in Figure 5 while Figure 6 shows an expanded view of the grid in the vicinity of the projectile. The computational domain extended to 4 body lengths in front, 4 body lengths in the radial direction and 4 body lengths behind the base of the projectile. The grid points in the normal direction were exponentially stretched away from the surface with the minimum spacing at the wall of $.00002D$. This spacing locates at least two points within the laminar sublayer.

The grid shown in Figure 6 was generated in two segments. First, the grid in the outer region is obtained using an elliptic solver¹³ for the ogive portion and straight-line rays for the remaining portion which extends to the downstream boundary. Second, the grid in the base region is obtained simply by extending the straight lines perpendicular to line AB down to the center line of symmetry (line CD). An exponential stretching with the minimum spacing of $.00002D$ at line AB is used. It should be noted that the same minimum spacing $.00002D$ is specified on both sides of the cut, thus maintaining a smooth variation of grid across the cut. This spacing could, of course, be increased downstream of the base. The number of grid points above and below line AB is the same (50 points) which means that an adequate number of points is located in the base region. As can be seen in Figure 6, the grid points are clustered near the nose-cylinder junction and at the projectile base where appreciable changes in flow variables are expected.

The free stream Reynolds number for the series of computations was fixed at 4.5×10^6 based on the total model length. The computations are started from free stream conditions and marched in time to obtain the steady state solution. The initial calculation was made for $M = 0.9$. Previous converged solutions were then used as starting conditions for additional Mach number runs to achieve faster convergence.

Figures 7 and 8 show the distribution of the surface pressure coefficient, C_p as a function of axial position, X/D . Figure 7 shows the overall view, whereas Figure 8 shows the distribution in the near wake region of the base. The distribution over the projectile surface itself is shown in both these figures. The value of C_p beyond $X/D = 6$ is the value of pressure coefficient along the cut AB. Both these figures indicate the shock waves near the nose-cylinder junction and near the blunt base. Although not shown

13. Steger, J.L., Nietubicz, C.J., and Heavey, K.R., "A General Curvilinear Grid Generation Program for Projectile Configurations," ARBRL-MR-03142, U.S. Army Ballistic Research Laboratory, ARRADCOM, Aberdeen Proving Ground, MD 21005, October 1981 (AD A107334).

in these figures, the pressure along the base remains fairly constant (within ± 0.005 variation in C_p values).

The series of Figures 9, 10 and 11 show the velocity vector field in the base region for $M = 0.9$ and $\alpha = 0$. Each vector shows the magnitude and the direction of the velocity at that point. Figure 9 shows the velocity field in the entire base region. One can see the expected velocity defect in the far wake region. Figures 10 and 11 show the velocity field in the vicinity of the base (near wake region), the difference between these two plots being that the former one is stretched (not drawn to same scale) while the latter is drawn with the same scale in x and y directions. Both figures clearly show the recirculation region of flow in the base region and indicate a strong shear layer as well.

The next two Figures 12 and 13 are stream function contour plots in the near wake region, again for $M = 0.9$ and $\alpha = 0$. Figure 13 is drawn to the same scale in x and y while Figure 12 is not. However, both of these figures are drawn to show the recirculation region and the position of the dividing stream line as clearly as possible. They also show the reattachment point which for this case is about 2 calibers down from the base.

A more critical check of the computational results is presented in Figure 14 where the base drag is plotted as a function of Mach number. Computational results are indicated by circles, experimental results⁷ by triangles and the squares indicate the results obtained using a semi-empirical technique developed by McCoy⁸. Base drag, as expected, increases as the Mach number increases from 0.9 to 1.2. The semi-empirical technique shows generally higher base drag when compared with computational and experimental results. The computational results predict the expected drag rise that occurs for $0.9 < M < 1.2$. The computational results, however, indicate a greater increase in drag than predicted by either the semi-empirical code or the experimental measurements. The discrepancy between the numerical and the experimental results should be anticipated since the experimental data were obtained with a sting attached to the base. The sting has an effect of weakening the recirculatory flow in the base region and leads to higher base pressure and hence, lower base drag.

As stated earlier, the present technique computes the entire flow field about the projectile including the base flow. Therefore, in addition to obtaining the base drag, the other drag components (pressure drag and skin friction drag) are computed as well. The three drag components can then be summed to determine the total aerodynamic drag. Figure 15 shows the variation of pressure drag with Mach number. As Mach number is increased from $M = .9$ to $M = 1.2$, shock waves form on the projectile surface and result in increasing pressure drag. In Figure 16 skin friction drag has been plotted as a function of Mach number and is shown to decrease as the Mach number increases from .9 to 1.2. Figure 17 shows the variation of total drag with Mach number and is compared with the available semi-empirical data. Both methods show the expected drag rise, typical of transonic flow over projectiles. The agreement is shown to vary throughout the transonic regime; however, this represents the first calculation of the total aerodynamic drag in a conceptually exact manner and thus is very encouraging.

V. SUMMARY

A procedure has been described in which the Azimuthal-Invariant (generalized axisymmetric) thin-layer Navier-Stokes code is modified in such a way as to compute the base flow field of projectiles at transonic speeds.

The computed results show the qualitative features of the flow field in the base region, namely the recirculation region, dividing stream line, reattachment point, etc. Quantitative comparisons of the base drag have been made with available data for various Mach numbers in the transonic speed range. These results indicate that the present numerical technique can be used to calculate the base drag of projectiles at transonic speeds.

The computed results for this paper represent the first application of thin-layer Navier-Stokes computational technique to predict projectile base flow at transonic velocity using the flow field segmentation described above. The results indicate that this technique shows good promise of providing a new and useful computational capability for exterior ballistics of shells.

Future computational efforts will investigate the implementation of viscous boundary condition on the projectile base, improved grid resolution, alternate turbulence models and supersonic flow.

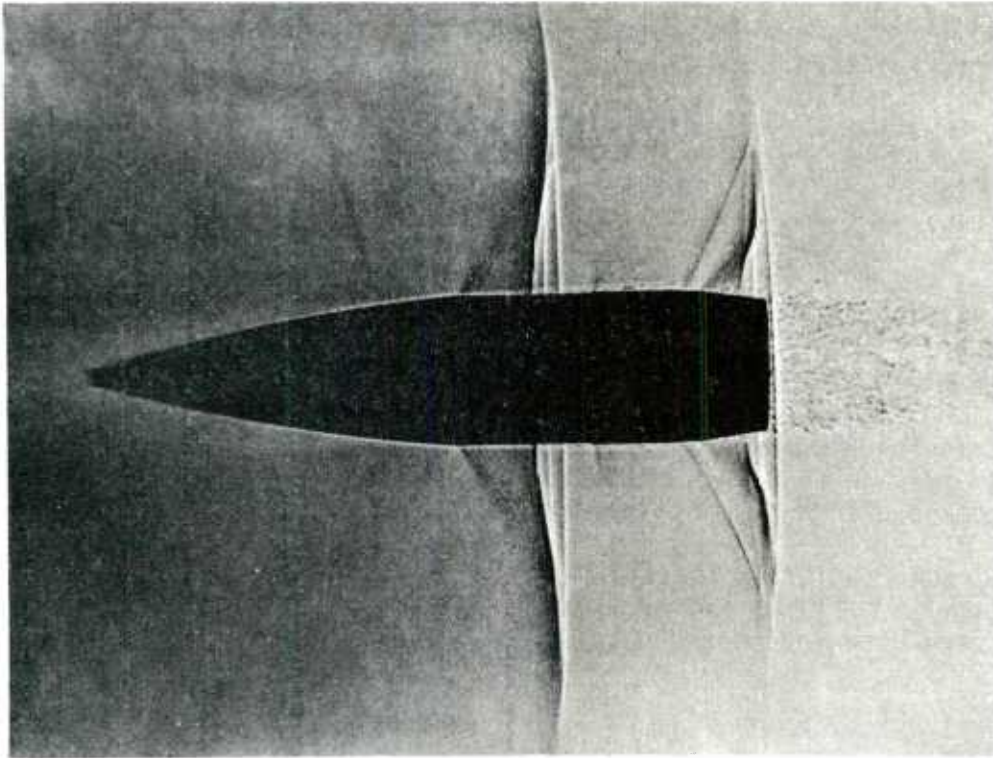


Figure 1. Spark Shadowgraph of Secant-Ogive-Cylinder-Boattail Projectile, $M = 0.95$, $\alpha \approx 0$

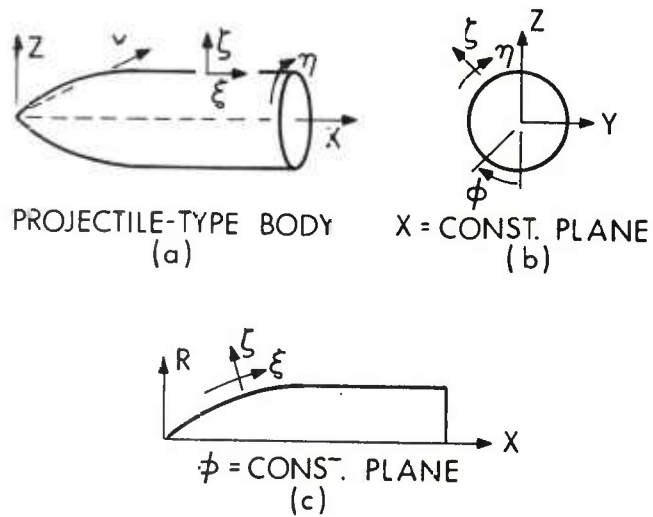


Figure 2. Axisymmetric Body and Coordinate System

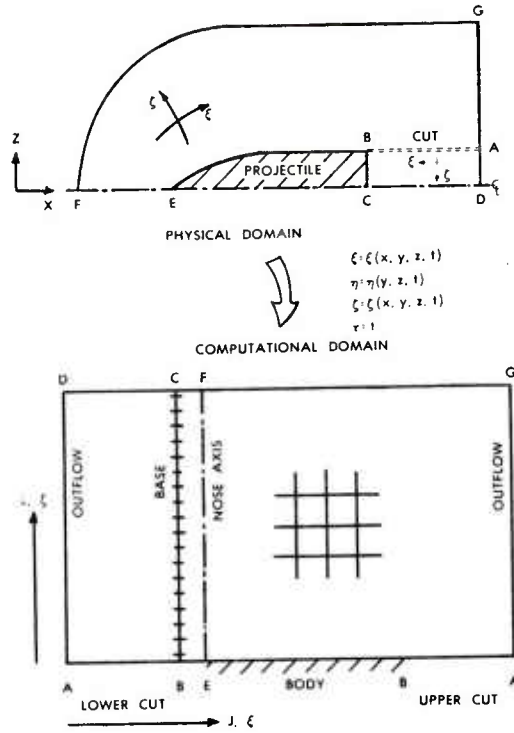
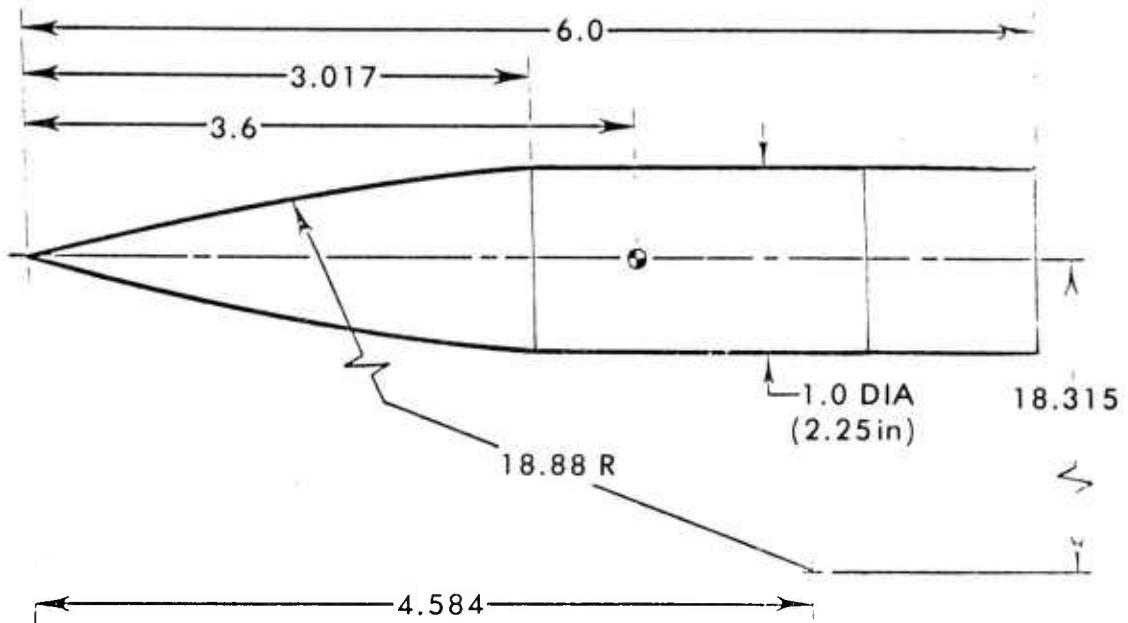


Figure 3. Schematic Illustration of Flow Field Segmentation



ALL DIMENSIONS IN CALIBERS

Figure 4. Model Geometry

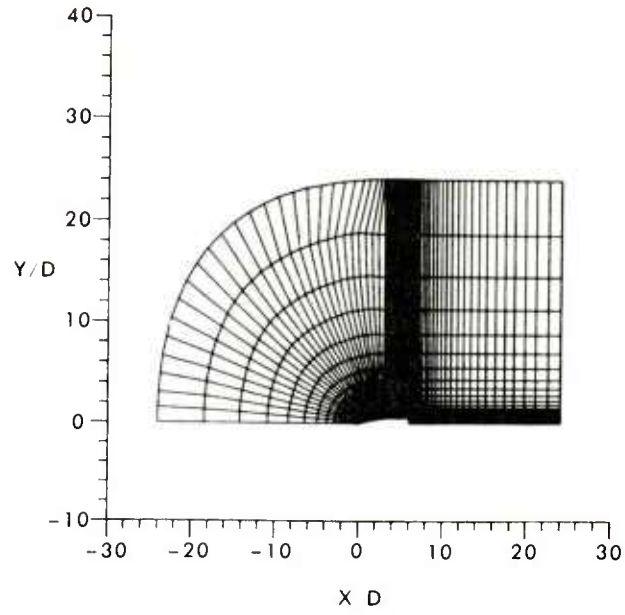


Figure 5. Computational Grid for Flow Field Computations

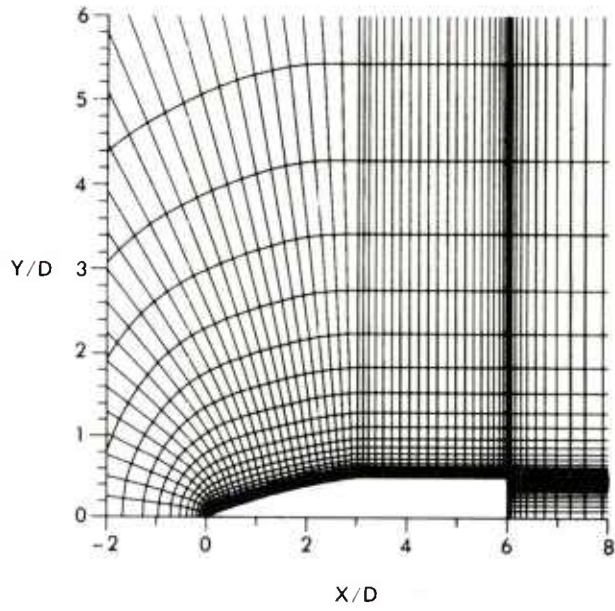


Figure 6. Expanded Grid

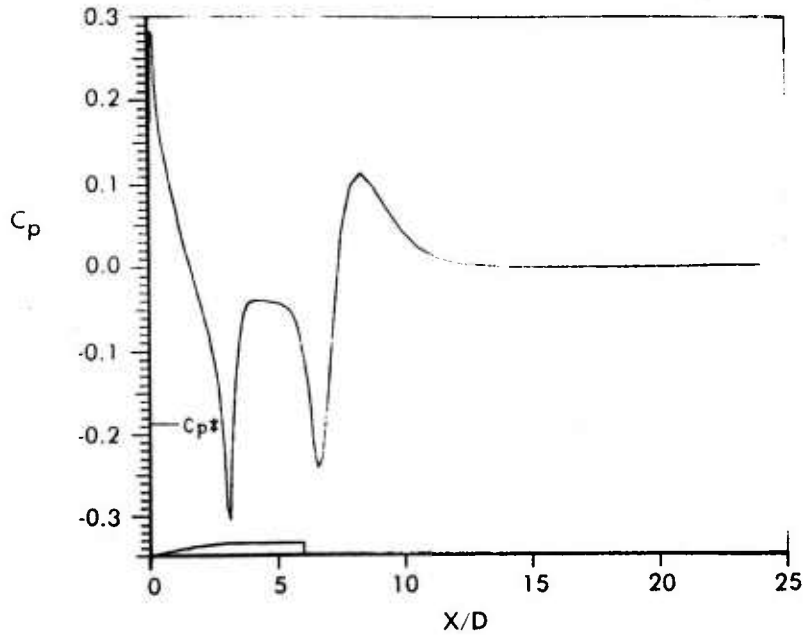


Figure 7. Longitudinal Surface Pressure Distribution, $M = 0.9$, $\alpha = 0$

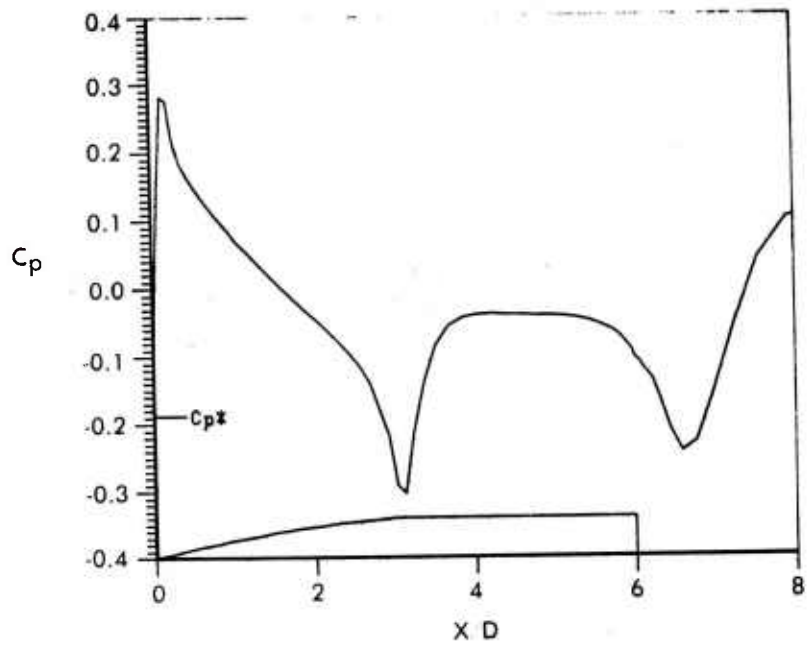


Figure 8. Longitudinal Surface Pressure Distribution, $M = 0.9$, $\alpha = 0$

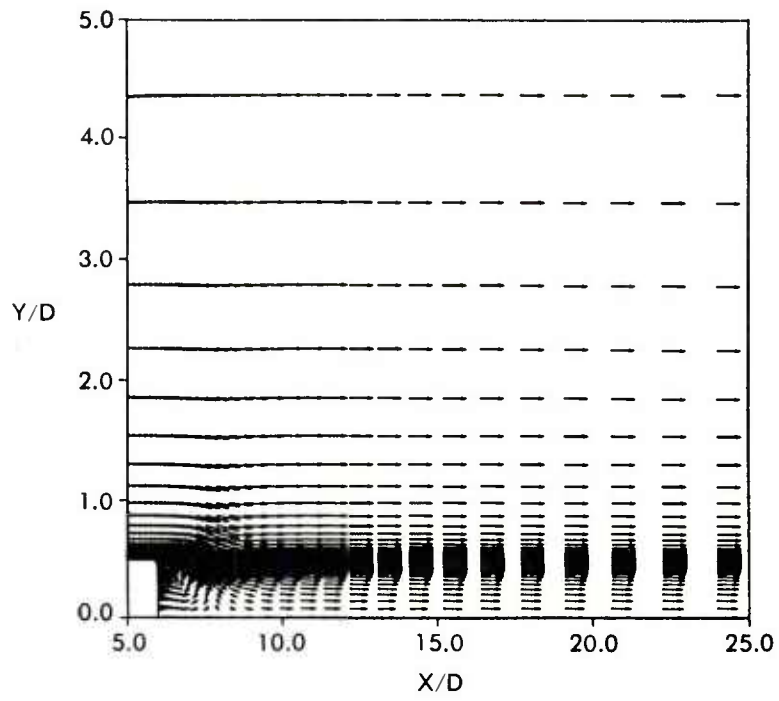


Figure 9. Velocity Vector Field, $M = 0.9$, $\alpha = 0$

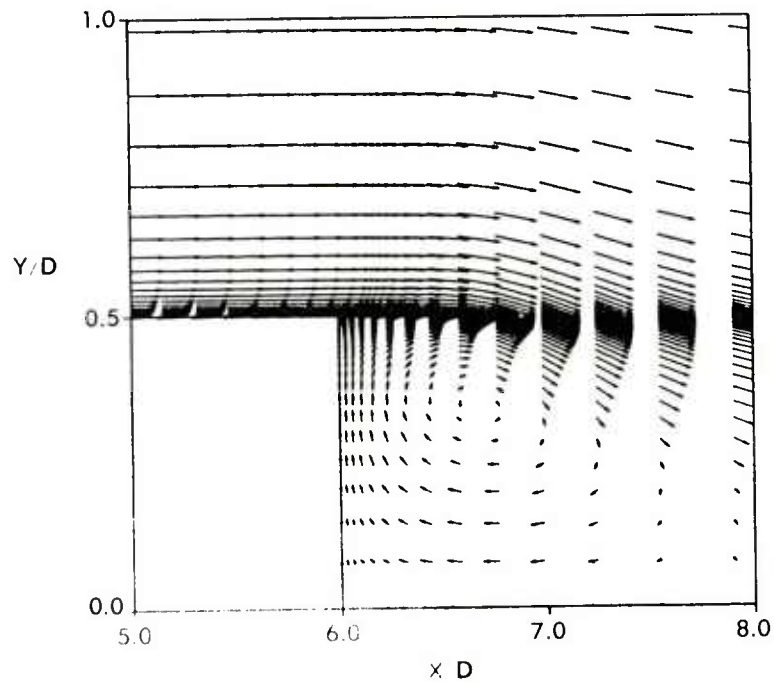


Figure 10. Velocity Vector Field, $M = 0.9$, $\alpha = 0$

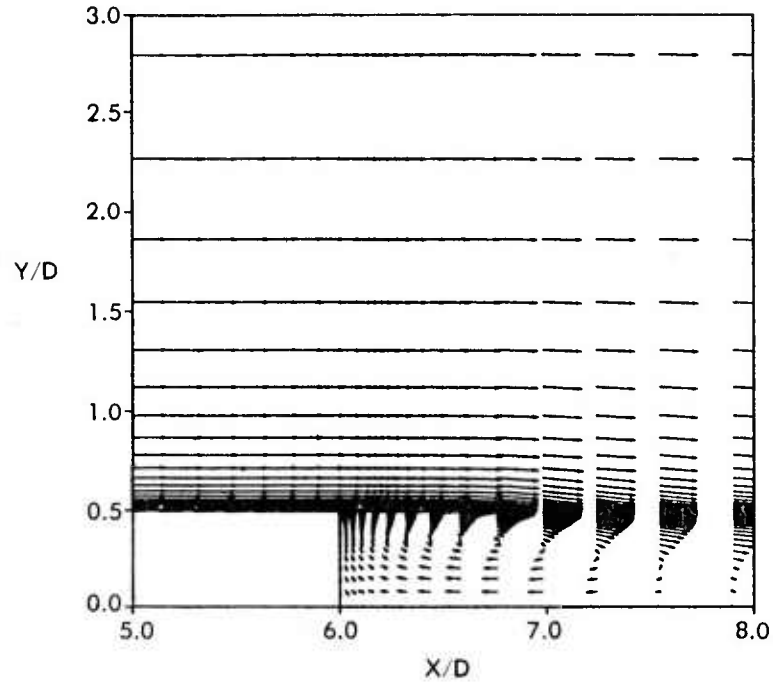


Figure 11. Velocity Vector Field, $M = 0.9$, $\alpha = 0$

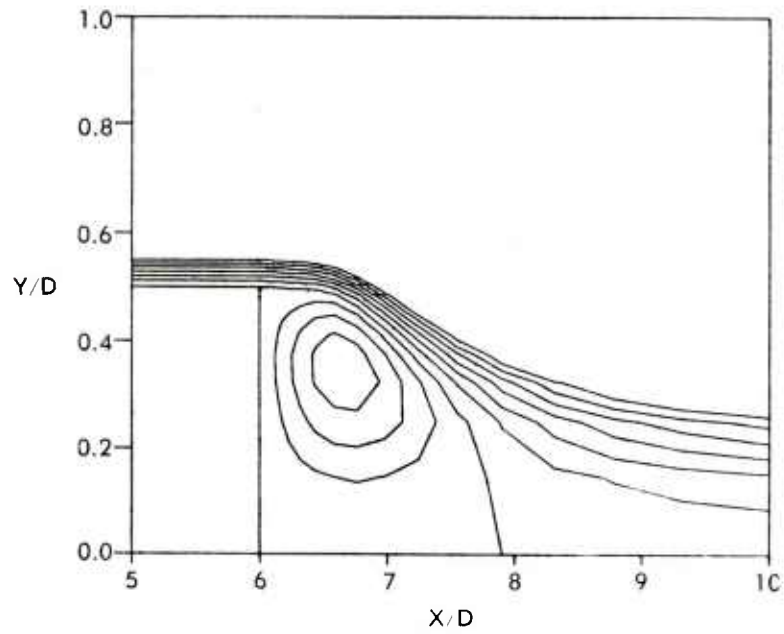


Figure 12. Stream Function Contours, $M = 0.9$, $\alpha = 0$

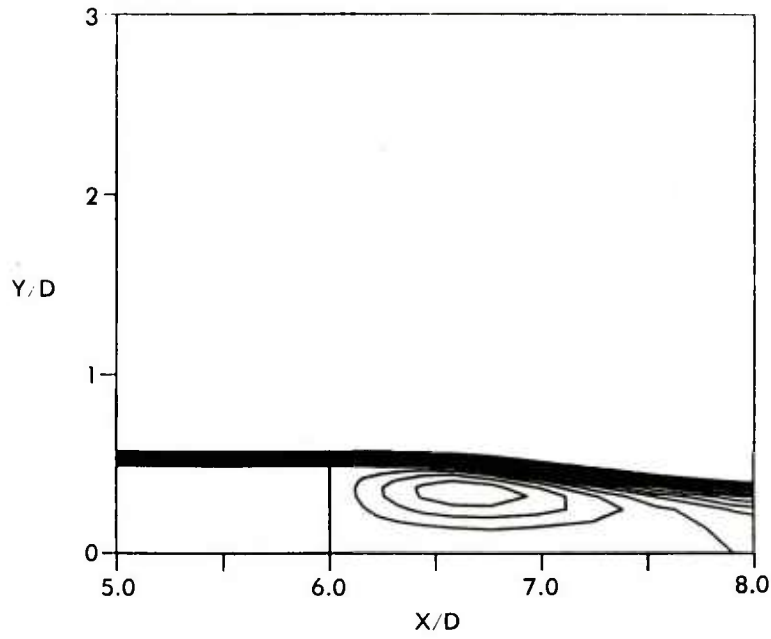


Figure 13. Stream Function Contours, $M = 0.9$, $\alpha = 0$

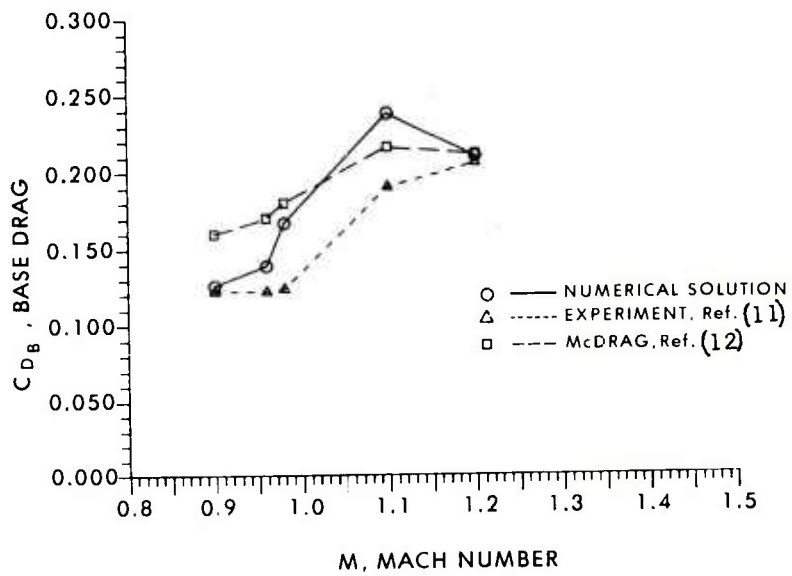


Figure 14. Variation of Base Drag Coefficient with Mach Number, $\alpha = 0$

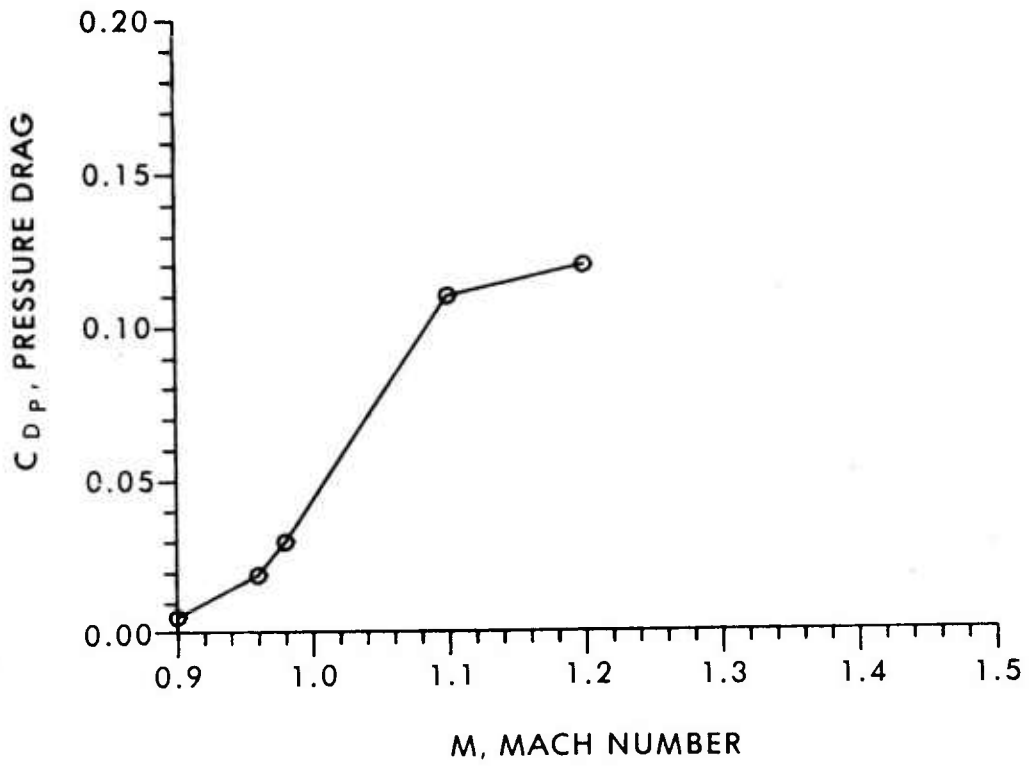


Figure 15. Variation of Pressure Drag Coefficient with Mach Number, $\alpha = 0$

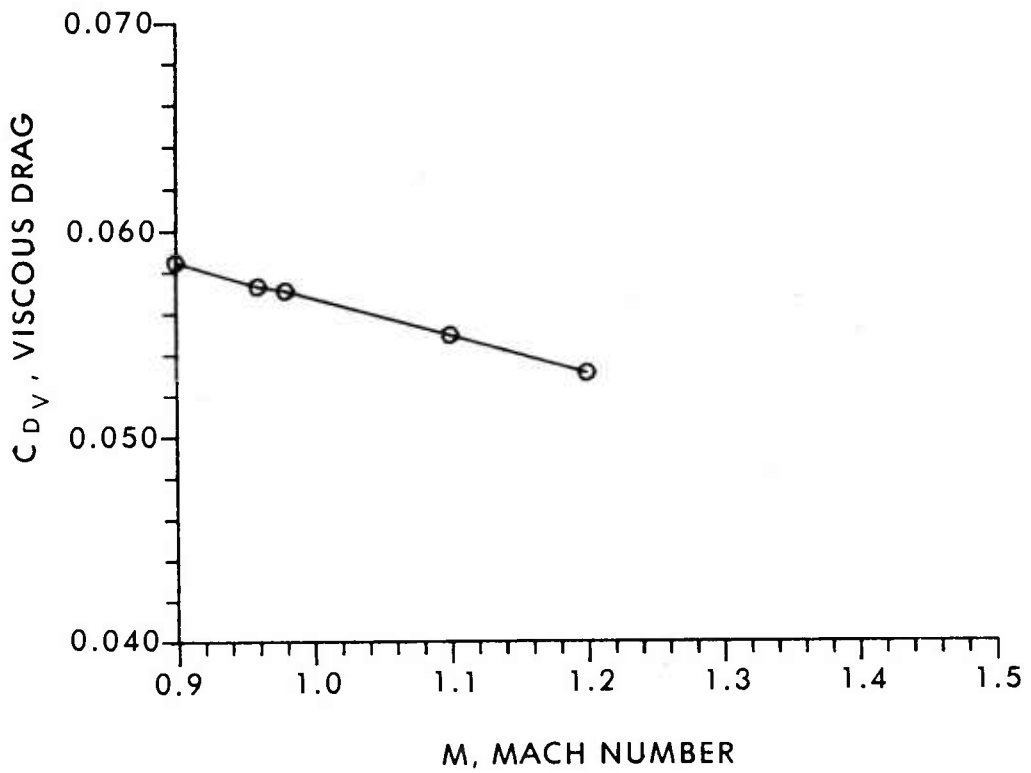


Figure 16. Variation of Viscous Drag Coefficient with Mach Number, $\alpha = 0$

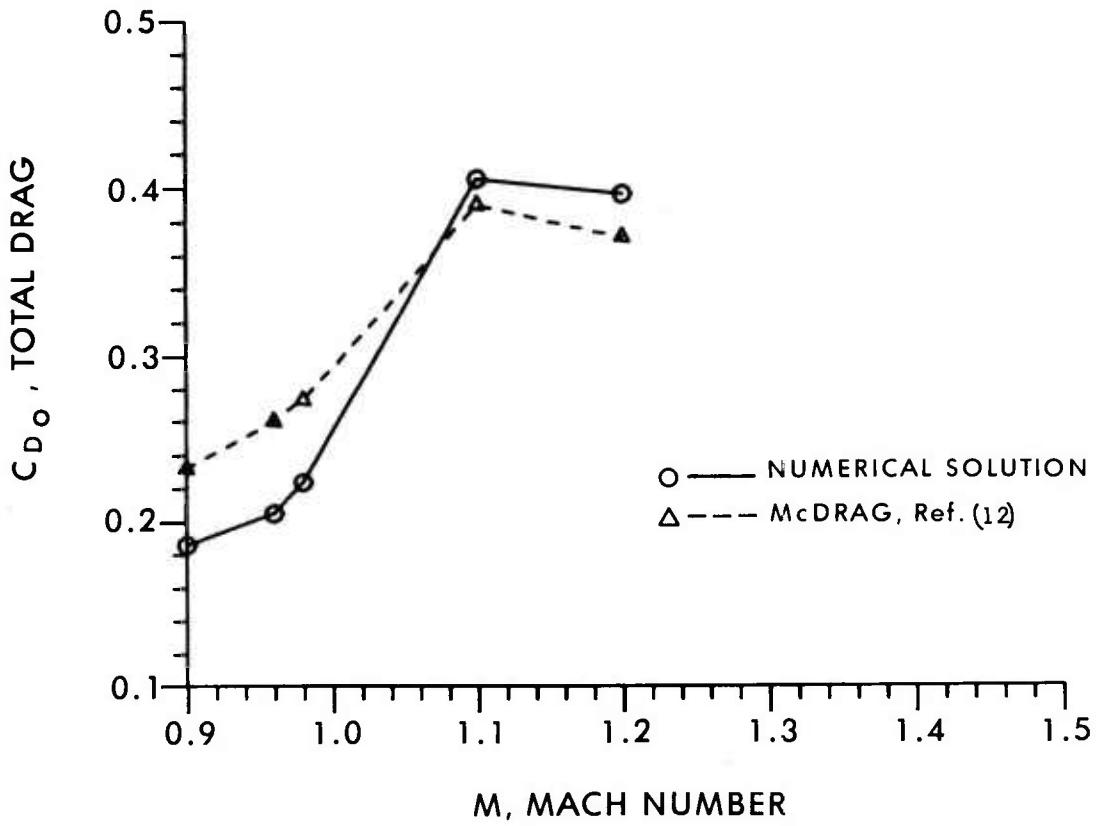


Figure 17. Variation of Total Drag Coefficient with Mach Number, $\alpha = 0$

REFERENCES

1. Nietubicz, C.J., Pulliam, T.H., and Steger, J.L., "Numerical Solution of the Azimuthal-Invariant Thin-Layer Navier-Stokes Equations," ARBRL-TR-02227, U.S. Army Ballistic Research Laboratory, ARRADCOM, Aberdeen Proving Ground, MD 21005, March 1980 (AD A085716).
2. Nietubicz, C.J., "Navier-Stokes Computations for Conventional and Hollow Projectile Shapes at Transonic Velocities," AIAA Paper No. 81-1262, June 1981.
3. Sedney, R., "Review of Base Drag," U.S. Army Ballistic Research Laboratory, ARRADCOM, Report No. 1337, Aberdeen Proving Ground, MD 21005, October 1966 (AD 808767).
4. Diewert, G.S., "A Computational Investigation of Supersonic Axisymmetric Flow over Boattails Containing a Centered Propulsive Jet," AIAA Paper No. 83-0462, January 10-13, 1983.
5. Weinberg, B.C., McDonald, H., and Shamroth, S.J., "Navier-Stokes Computations of Aft End Flow Fields," Final Report, Army Research Office Contract DAAG29-79-C-0003, May 1982.
6. Chow, W.L., Bober, L.J., and Anderson, B.H., "Strong Interaction Associated with Transonic Flow Past Boattails," AIAA Journal, Vol. 13, No. 1, 1975, pp. 112-113.
7. Baldwin, B.S., and Lomax, H., "Thin-Layer Approximation and Algebraic Model for Separated Turbulent Flows," AIAA Paper No. 78-257, 1978.
8. Beam, R., and Warming, R.F., "An Implicit Factored Scheme for the Compressible Navier-Stokes Equations," AIAA Paper No. 77-645, June 1977.
9. Steger, J.L., "Implicit Finite Difference Simulation of Flow About Arbitrary Geometries with Application to Airfoils," AIAA Journal, Vol 16, No. 4, July 1978, pp. 679-686.
10. Pulliam, T.H., and Steger, J.L., "On Implicit Finite-Difference Simulations of Three-Dimensional Flow," AIAA Journal, Vol. 18, No. 2, February 1980, pp. 159-167.
11. Kayser, L.D., "private communications," Ballistic Research Laboratory, Aberdeen Proving Ground, MD 21005.
12. McCoy, R.L., "McDrag - A Computer Program for Estimating the Drag Coefficients of Projectiles," ARBRL-TR-02293, U.S. Army Ballistic Research Laboratory, ARRADCOM, Aberdeen Proving Ground, MD 21005, February 1981 (AD A098110).
13. Steger, J.L., Nietubicz, C.J., and Heavey, K.R., "A General Curvilinear Grid Generation Program for Projectile Configurations," ARBRL-MR-03142, U.S. Army Ballistic Research Laboratory, ARRADCOM, Aberdeen Proving Ground, MD 21005, October 1981 (AD A107334).

LIST OF SYMBOLS

a	speed of sound
A	cross sectional area at the base
C_{D_b}	base drag coefficient, $2 D_b / \rho_\infty u_\infty^2 A$
c_p	specific heat at constant pressure
C_p	pressure coefficient, $2(p - p_\infty) / \rho_\infty a_\infty^2$
D	body diameter (57.15mm)
D_b	base drag
e	total energy per unit volume / $\rho_\infty a_\infty^2$
\hat{q}	vector of dependant variables in transformed equations
\hat{E}, \hat{F}	flux vector of transformed Navier-Stokes equations
\hat{H}	η -invariant source vector
J	Jacobian of transformation
M	Mach number
p	pressure / $\rho_\infty a_\infty^2$
Pr	Prandtl number, $\mu_\infty C_p / \kappa_\infty$
R	body radius
Re	Reynolds number, $\rho_\infty a_\infty D / \mu_\infty$
\hat{S}	viscous flux vector
t	physical time
u,v,w	Cartesian velocity components / a_∞
U,V,W	Contravariant velocity components / a_∞
x,y,z	physical Cartesian coordinates
α	angle of attack
γ	ratio of specific heats
κ	coefficient of thermal conductivity
μ	coefficient of viscosity

LIST OF SYMBOLS (continued)

ξ, η, ζ transformed coordinates in axial, circumferential and radial directions

ρ density/ ρ_∞

τ transformed time

φ circumferential angle

Superscript

* critical value

Subscript

b base

p pressure

v viscous

∞ free stream conditions

DISTRIBUTION LIST

<u>No. of Copies</u>	<u>Organization</u>	<u>No. of Copies</u>	<u>Organization</u>
12	Administrator Defense Technical Info Center ATTN: DTIC-DDA Cameron Station Alexandria, VA 22314	1	Director US Army Air Mobility Research and Development Laboratory Ames Research Center Moffett Field, CA 94035
1	Commander US Army Materiel Development and Readiness Command ATTN: DRCMDM-ST 5001 Eisenhower Avenue Alexandria, VA 22333	1	Commander US Army Communications Rsch and Development Command ATTN: DRSEL-ATDD Fort Monmouth, NJ 07703
8	Commander US Army Armament Research and Development Command ATTN: DRDAR-TDC DRDAR-TSS DRDAR-LCA-F Mr. D. Mertz Mr. A. Loeb Mr. S. Wasserman Mr. H. Hudgins Mr. E. Friedman Dover, NJ 07801	1	Commander US Army Electronics Research and Development Command Technical Support Activity ATTN: DELSD-L Fort Monmouth, NJ 07703
1	Commander US Army Armament Materiel Readiness Command ATTN: DRSAR-LEP-L Rock Island, IL 61299	2	Commander US Army Missile Command ATTN: DRSMI-R DRSMI-RDK Mr. R. Deep Redstone Arsenal, AL 35898
1	Director US Army Armament Research and Development Command Benet Weapons Laboratory ATTN: DRDAR-LCB-TL Watervliet, NY 12189	1	Commander US Army Missile Command ATTN: DRSMI-YDL Redstone Arsenal, AL 35898
1	Commander US Army Aviation Research and Development Command ATTN: DRDAV-E 4300 Goodfellow Blvd. St. Louis, MO 63120	1	Commander US Army Tank Automotive Command ATTN: DRSTA-TSL Warren, MI 48090
		1	Director US Army TRADOC Systems Analysis Activity ATTN: ATAA-SL White Sands Missile Range NM 88002
		1	Commander US Army Research Office P. O. Box 12211 Research Triangle Park NC 27709

DISTRIBUTION LIST

<u>No. of Copies</u>	<u>Organization</u>	<u>No. of Copies</u>	<u>Organization</u>
1	Commander US Naval Air Systems Command ATTN: AIR-604 Washington, D. C. 20360	2	Sandia Laboratories ATTN: Division No. 1331, Mr. H.R. Vaughn Mr. G.R. Eisler Albuquerque, NM 87115
4	Commander US Naval Surface Weapons Center ATTN: Dr. T. Clare, Code DK20 Dr. P. Daniels Mr. D. A. Jones III Mr. L. Mason Dahlgren, VA 22448	1	AEDC Calspan Field Services ATTN: MS 600 (Dr. John Benek) AAFS, TN 37389
3	Commander US Naval Surface Weapons Center ATTN: Code 312 Dr. C. Hsieh Dr. W. Yanta Mr. R. Voisinet Silver Spring, MD 20910	1	Stanford University Department of Aeronautics and Astronautics ATTN: Prof. J. Steger Stanford, CA 94305
1	Commander US Naval Weapons Center ATTN: Code 3431, Tech Lib China Lake, CA 93555	1	University of California, Davis Department of Mechanical Engineering ATTN: Prof. H.A. Dwyer Davis, CA 95616
1	Director NASA Langley Research Center ATTN: NS-185, Tech Lib Langley Station Hampton, VA 23365	1	University of Delaware Mechanical and Aerospace Engineering Department ATTN: Dr. J. E. Danberg Newark, DE 19711
2	Commandant US Army Infantry School ATTN: ATSH-CD-CSO-OR Fort Benning, GA 31905	1	University of Maryland Dept. of Aerospace Engineering ATTN: Dr. J. D. Anderson, Jr. College Park, MD 20742
3	Director NASA Ames Research Center ATTN: MS-202A-14, Dr. P. Kutler MS-202-1, Dr. T. Pulliam MS-227-8, Dr. L. Schiff Moffett Field, CA 94035	1	University of Illinois at Urbana Champaign Department of Mechanical and Industrial Engineering ATTN: Prof. W. L. Chow Urbana, IL 61801

DISTRIBUTION LIST

<u>No. of Copies</u>	<u>Organization</u>
1	University of Notre Dame Department of Aeronautical and Mechanical Engineering ATTN: Prof. T. J. Mueller Notre Dame, IN 46556
1	University of Texas-Austin Department of Aerospace Engineering ATTN: Dr. J. J. Bertin Austin, TX 78712

Aberdeen Proving Ground

Dir, USAMSAA
ATTN: DRXSY-D
DRXSY-MP, H. Cohen

Cdr, USATECOM
ATTN: DRSTE-TO-F

Dir, USACSL, Bldg. E3516, EA
ATTN: DRDAR-CLB-PA
DRDAR-CLN
DRDAR-CLJ-L

USER EVALUATION OF REPORT

Please take a few minutes to answer the questions below; tear out this sheet, fold as indicated, staple or tape closed, and place in the mail. Your comments will provide us with information for improving future reports.

1. BRL Report Number _____
2. Does this report satisfy a need? (Comment on purpose, related project, or other area of interest for which report will be used.)

3. How, specifically, is the report being used? (Information source, design data or procedure, management procedure, source of ideas, etc.) _____

4. Has the information in this report led to any quantitative savings as far as man-hours/contract dollars saved, operating costs avoided, efficiencies achieved, etc.? If so, please elaborate.

5. General Comments (Indicate what you think should be changed to make this report and future reports of this type more responsive to your needs, more usable, improve readability, etc.) _____

6. If you would like to be contacted by the personnel who prepared this report to raise specific questions or discuss the topic, please fill in the following information.

Name: _____

Telephone Number: _____

Organization Address: _____
